01 Jan 2010

Energy Harvesting from Vibration with Alternate Scavenging Circuitry and Tapered Cantilever Beam

Shahab Mehraeen

Jagannathan Sarangapani
Missouri University of Science and Technology, sarangap@mst.edu

Keith Corzine
Missouri University of Science and Technology

Recommended Citation

S. Mehraeen et al., "Energy Harvesting from Vibration with Alternate Scavenging Circuitry and Tapered Cantilever Beam," *IEEE Transactions on Industrial Electronics*, Institute of Electrical and Electronics Engineers (IEEE), Jan 2010.
The definitive version is available at https://doi.org/10.1109/TIE.2009.2037652

Energy Harvesting From Vibration With Alternate Scavenging Circuitry and Tapered Cantilever Beam

Shahab Mehraeen, *Student Member, IEEE*, S. Jagannathan, *Senior Member, IEEE*, and Keith A. Corzine, *Senior Member, IEEE*

***Abstract*—Piezoelectric transducers are increasingly being used to harvest energy from environmental vibrations in order to either power remote sensors or charge batteries that power the sensors. In this paper, a new voltage compensation scheme for high-voltage-based (> 100 V) energy harvesting is introduced, and its fundamental concepts, as well as the operation details, are elaborated. This scheme, when applied to the voltage inversion method [synchronized switch harvesting on inductor (SSHI)], provides an increase of over 14% in harvested power when compared to the parallel inversion method (parallel SSHI) alone and more than 50% in the case of series inversion method (series SSHI). Second, tapered cantilever beams were shown to be more effective in generating a uniform strain profile over rectangular and trapezoidal beams if they are precisely shaped, resulting in a significant increase in harvested power over available methods in the literature from laboratory experimental tests. In addition, a simplified method to design such a beam is introduced. Finally, a field test of the proposed tapered beam is conducted by using a dozer for earth-moving applications, and experimental results are discussed.**

***Index Terms*—Cantilever beam, energy harvesting, piezoelectric.**

I. Introduction

In RECENT years, there appears to be a significant demand to utilize environmental energy for both high-power [1], [2] and low-power devices [3] such as wearable devices, wireless sensors, and portable electronic devices due to their need in remote sensing and embedded prognostic application environments [4]. As wireless devices are becoming a necessity in numerous monitoring and prognostic applications, batteries have been the main power source in these devices. However, in applications for which continuous data gathering is essential, such as sensors that monitor remote structures in earth-moving equipment and bridges [5], the periodic maintenance procedure for batteries is labor intensive, costly, and tedious.

Scavenging energy from the environment, also known as "energy harvesting," is defined as the conversion of ambient energy into a usable electrical form. The collected energy from the environment is either sufficient to power a remote sensor or at least is able to extend the rechargeable battery lifetime. In addition, small wireless sensors which typically use tiny batteries [6] will not survive long-term usage unless the batteries are impractically larger than the sensing and processing hardware even for low-consumption applications. By using energy harvesting, the battery pack can be made either significantly small or removed [7].

Among available energy-harvesting methodologies, piezoelectric transducer (PZT)-based approach was chosen because of abundant vibration accessibility and energy-harvesting productivity of piezoelectric materials [4], [8]. Other approaches include solar, thermal, electromagnetic, electrostatic, and so on.

The direct connection of the load to the piezoelectric material is not generally recommended in piezoelectric energy harvesting. An efficient energy-harvesting mechanism consists of a piezoelectric material bonded to a cantilever beam, voltage inversion circuitry [also known as synchronized switch harvesting on inductor (SSHI)] [9], [10], rectifier, power converter for conditioning, and load. It has been shown [11]–[13] that, by using a power converter for conditioning the voltage, the scavenged power from a piezoelectric material can be increased. Consequently, different voltage inversion techniques have been proposed to shape the generated voltage in order to increase both the voltage and the power factor so as to enhance the harvested power [9], [10], knowing that the piezoelectric material acts as a current source in the presence of sustained vibration.

Though the shaped voltage increases the harvested power noticeably, it does not result to the highest average voltage value needed for harvesting the maximum power. Therefore, in [14], a new scheme, along with some preliminary results, is introduced to shape the voltage in order to achieve the maximum average voltage value in piezoelectric-based power harvesting. By contrast, in this paper, a detailed theoretical analysis of this new scheme and more elaborated results from the lab experiments are included. In addition, field evaluation is added.

In PZT-based energy harvesting, different mechanical structures have been presented [15]–[17] to transfer the vibration energy to the piezoelectric material. Among these, the cantilever beam is more attractive for its relatively low resonance frequency and high average strain for a given input force [15]. However, the existing cantilever-beam-based schemes [15] do not produce a uniform strain distribution (with maximum tolerable strain value) along the beam, and consequently, they do not generate the maximum energy from vibration. Thus, a tapered beam design is introduced [14] in order to provide

Manuscript received August 20, 2008; revised November 19, 2009. First published December 4, 2009; current version published February 10, 2010. This work was supported in part by the National Science Foundation Center on Intelligent Maintenance Systems under Grant ECCS#0624644.

The authors are with the Department of Electrical and Computer Engineering, Missouri University of Science and Technology, Rolla, MO 65409 USA (e-mail: sm347@mst.edu; sarangap@mst.edu; Keith@Corzine.net).

Digital Object Identifier 10.1109/TIE.2009.2037652

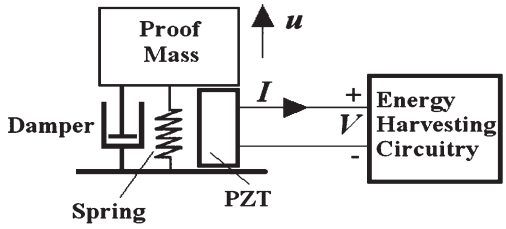

Fig. 1. Piezoelectric under mechanical vibration.

a uniform strain profile to increase the harvested power; a simplified version of which is presented herein. Moreover, in the following, new experimental lab results, as well as field test evaluations, are presented, which were not included in [14] before providing concluding remarks.

II. Proposed Voltage Compensation Scheme

Before presenting the voltage compensation scheme, a vibrating piezoelectric (PZT) device can be modeled as a current source in parallel to a capacitor which represents its internal impedance. Under sinusoidal vibration, the material electrical characteristics can be transformed into a more convenient form [9] as $I = i_P - C_P\dot{V}$, where I is the output current, $i_p = I_P \sin(\omega t)$ is the PZT polarization current with a peak value given by I_P, ω is the vibration angular frequency, C_P is the PZT capacitance (clamped capacitor), and V is the PZT terminal voltage.

The piezoelectric polarization current can be calculated by using $i_P = \alpha\dot{u}$ [9], where α is the force factor which is a function of the piezoelectric parameters, as well as the mechanical structure geometry, and u is the displacement of the proof mass according to Fig. 1.

Thus, in a constant vibration environment (frequency and amplitude) where mechanical motion is sinusoidal, I_P can be considered as a constant. In addition, if the generated voltage is low in the presence of constant current, low power is harvested. In all the voltage inversion techniques described in [9] and [10], due to the dissipations involved in the switching hardware that is typically built using solid-state switches and inductors, the magnitude of the output voltage is less than what it would be in a lossless inversion. In high-voltage applications with voltages greater than 100 V (in contrast with [7]–[12] where the voltage ranges from 1 to 70 V), the voltage drop is quite high because of higher switching and inductor core losses. To mitigate the losses, the following method is introduced to increase the scavenged power in a voltage inversion technique.

The proposed scheme charges the internal capacitor of the piezoelectric material after each voltage inversion in order to increase the voltage level. As a consequence, some energy is required to raise the voltage in the material, as well as to overcome the dissipation due to the direct charging of the PZT capacitor. Despite this energy requirement, with the proposed scheme, the net output energy of the scavenger, which is the output energy minus the mentioned consumptions, is much higher than the case when the voltage inversion technique is used alone (i.e., voltage inversion without the proposed scheme).

In the following sections, the main ideas in the proposed scheme are first discussed, wherein it will be shown that the piezoelectric voltage level (and the harvested energy) will be increased as a result of voltage compensation and the amount of the dissipated energy involved in the voltage compensation can be reduced using the proposed scheme.

A. Fundamental Concepts

In a typical series RC circuit connected to a step voltage source V_s, it can be shown that, by charging the capacitor in multiple equal voltage steps, the dissipated energy through the resistor is reduced by a factor of number of steps. We assume that the capacitor is charged from a voltage V_1 to a higher voltage of V_2; thus, $\Delta V_S = V_2 - V_1$. By solving $V_2 = RC\dot{V}_C + V_C$, the capacitor voltage becomes $V_C = (V_1 - V_2)e^{-t/RC} + V_2$. Then, the resistor current is obtained as $I_R = C\,dV_C/dt = (\Delta V_S/R)e^{-t/RC}$; thus, the dissipated power in the path resistor R can be calculated as $P_R = RI_R^2 = ((\Delta V_S)^2/R)e^{-2t/RC}$. By taking the integral of the dissipated power, the amount of dissipated energy is obtained as

$$W_{\rm DISS} = \int_0^\infty P_R\,dt = \left[-\frac{RC}{2}\frac{(\Delta V_S)^2}{R}\,e^{-2t/RC}\right]_0^\infty = \frac{C}{2}(\Delta V_S)^2. \tag{1}$$

Equation (1) reveals that the amount of dissipated energy is independent of the path resistor. Now, assume that charging from V_1 to V_2 is accomplished in α number of equally spaced voltage steps satisfying

$$\Delta V_S = \sum_{i=1}^{\alpha} \Delta V_{Si}, \qquad \Delta V_{Si} = \Delta V_{Sj}; \quad 1 \le i \le \alpha; \quad 1 \le j \le \alpha. \tag{2}$$

By using (1) and (2), the total dissipated energy in the new scenario is calculated as

$$E_{\rm DISS} = \frac{C}{2}\sum_{i=1}^{\alpha}(\Delta V_{Si})^2 = \frac{\alpha C}{2}(\Delta V_{Si})^2, \qquad 1 \le i \le \alpha. \tag{3}$$

From (1), the total dissipated energy in the voltage step $\Delta V_S = \alpha\Delta V_{Si}$ is equal to

$$W_{\rm DISS} = \frac{C}{2}(\alpha\Delta V_{Si})^2, \qquad 1 \le i \le \alpha. \tag{4}$$

Comparing (3) and (4), we obtain $E_{\rm DISS} = W_{\rm DISS}/\alpha$. This, in turn, results in the piezoelectric direct charging dissipation as

$$E_{\rm DISS} = \frac{C}{2\alpha}(\Delta V_S)^2 = \frac{1}{2\alpha}C_p(V_2 - V_1)^2. \tag{5}$$

Otherwise, when equal voltage steps are not used, the dissipations will be higher than in (5). Assume that the voltage $\Delta V_S = \beta\Delta V_S + (1-\beta)\Delta V_S$ is split into two arbitrary steps

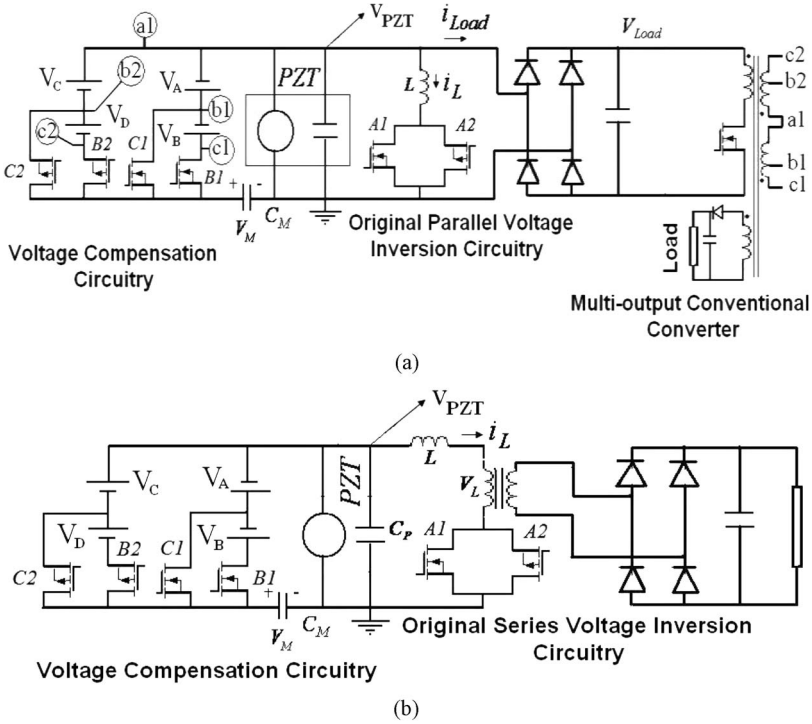

Fig. 2. (a) Parallel voltage compensation topology. (b) Series voltage compensation topology [14]. The capacitor C_M is added for measuring the transferred charge to PZT in compensating stages and is not part of the topology.

with $\beta \leq 1$. Then, $E_{\rm DISS} = C(\Delta V_S)^2(2\beta^2 - 2\beta + 1)/2$ has a minimum at $\beta = 1/2$. This reasoning can be easily extended to more numbers of steps. Thus, equal steps yield minimum loss.

Although (1) suggests an infinite time interval to calculate the path dissipation, a finite upper bound can be used, provided that the time constant RC_P is small enough. In our lab tests, the time constant $RC_P < 10$ μs renders an error that is less than 0.01% in the dissipated energy calculation when the time interval is $5RC_P$. This time is significantly smaller than the vibration intervals with a frequency range of 50–100 Hz encountered in the application environments.

B. Voltage Compensation in Parallel Inversion Technique

Fig. 2(a) shows the two-stage voltage compensation topology [14]. Here, switches $B1$ and $C1$ are synchronized with switch $A1$, where they turn on sequentially, as will be described. According to Fig. 3(a), when the polarization current $i_p = I_P \sin(\omega t)$ turns negative, the original voltage inversion circuitry is activated and inverts the PZT voltage $V_{\rm PZT}$ through the switching circuit consisting of switch $A1$ and inductor L and decreases the voltage from V_2 to $-V_1$. After the inversion time, which, according to Fig. 3(a), is equal to $\pi\sqrt{LC_P}$ [9], [14], switch $C1$ is closed and decreases the PZT voltage to $-V_3 = -(V_1 + (V_2 - V_1)/2)$ [see Fig. 3(a)]. Switch $C1$ stays closed until the new voltage $-V_3$ builds ($t_1 = 5R_1C_P$, where R_1 is the $C1$ to C_P loop resistance). Next, switch $B1$ is closed and decreases the PZT voltage to $-V_2$, where the PZT voltage is measured with respect to the circuit ground shown in Fig. 2(a). Similar to switch $C1$, switch $B1$ is opened after $t_2 = 5R_2C_P$ (with R_2 being the $B1$ to C_P loop resistance), and the piezoelectric polarization current source starts to transfer charge to the clamped capacitor. Time delays (t_1 and t_2) around 50 μs are easily achievable in the lab environment.

Shorter delays can be achieved through the selection of fast switches. It should be noted that the total delay corresponding to inversion and compensation steps must be a small fraction of the vibration period such that the piezoelectric scavenger is able to collect energy under the highest voltage almost continuously. The voltage steps are shown in Fig. 3(a) as $C1$ and $B1$. In the actual circuit, each switch is accompanied by a series diode to prevent current in the wrong direction. Similarly, switches $B2$ and $C2$ are synchronized with switch $A2$ in the same way for the positive polarization current, where $V_{\rm PZT}$ is increased from $-V_2$ to V_1 by the original voltage inversion circuit. Then, it is further increased to $V_1 + (V_2 - V_1)/2$ and V_2 by switches $C2$ and $B2$, respectively. The procedure for positive polarization current is shown and encircled in Fig. 3(a) for the case of parallel voltage compensation. The voltage compensation switches $B1$, $C1$, $B2$, and $C2$ allow the transfer of energy to the piezoelectric clamped capacitor in two equal voltage steps, thus increasing the voltage level in each half cycle of i_p ($T/2 = \pi/\omega$).

Increasing the number of stages provides more voltage steps and, consequently, less dissipation, as well as more net output power, as described before; however, it results in more complex circuitry. It is shown in [11] that a power converter is needed to deliver the power from PZT to the low-voltage load; thus, a multioutput converter can be utilized to provide the compensation voltages, as well as load voltage. Typical piezoelectric waveforms during voltage inversion are shown in Fig. 3(a) for this topology. Next, a power analysis in the voltage compensation scheme is introduced.

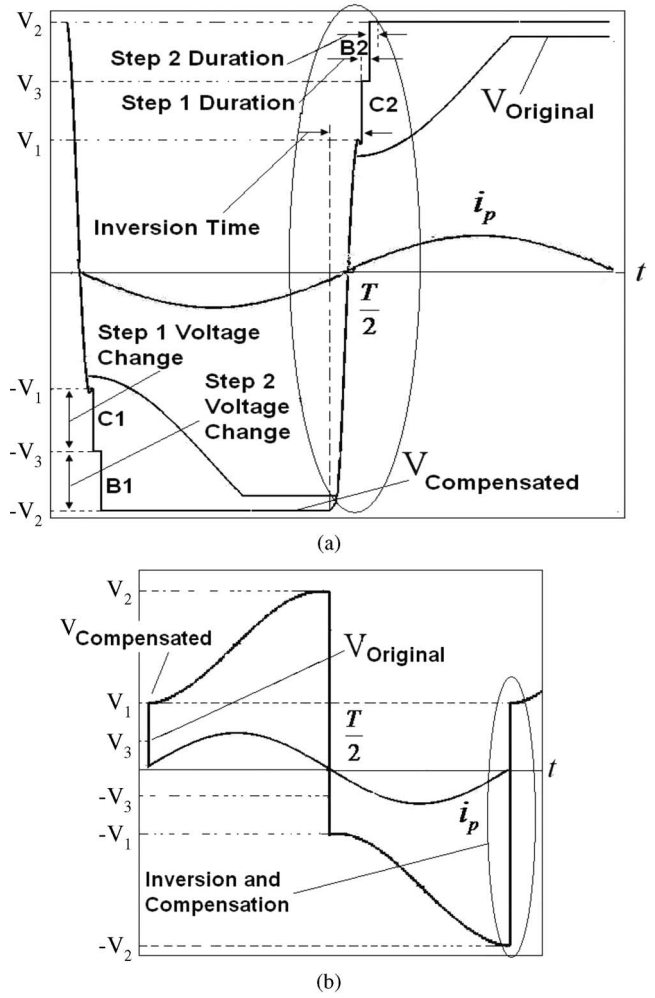

Fig. 3. (a) PZT voltage $V_{\rm PZT}$ waveforms in the original parallel voltage inversion technique and in voltage compensation scheme with two-step compensation. (b) Voltage levels in series voltage compensation scheme.

C. Power Calculation in Voltage Compensation Scheme

The generated PZT power depends on the magnitude of current, voltage, and power factor (or the phase between the current and the voltage.) Since the piezoelectric material acts as a current source in the presence of sustained vibration, its magnitude is dependent upon the magnitude of vibration. Conventional converters, which help decrease the current–voltage phase difference (power factor increase), have been utilized to increase the harvested power. In [12], by employing the adaptive control of dc–dc converter, the piezoelectric output impedance is matched with load impedance dynamically, whereas in [13], the impedance of the transducer was adjusted by using the multilayer technology of the material together with an electrical circuitry. In [9], [10], and [18], on the other hand, the harvested power is increased via synchronizing the PZT current and voltage (maximizing the power factor) through the voltage inversion technique where a practical low-consumption inversion circuitry is also proposed. By contrast, in this paper, by using the proposed voltage compensation scheme, the PZT-generated power is attained by increasing the voltage level in addition to maximizing the power factor.

Two key features can be obtained by using the proposed scheme. First, the piezoelectric voltage is increased by means of direct charging of PZT-clamped capacitor when the polarization current is zero; thus, the voltage after inversion is increased (compensated) since the inversion process [9], [10] drops the voltage significantly in high-voltage applications due to switching and inductor losses [see $|V_1|$ and $|V_2|$ in Fig. 3(a)]. Second, the proposed procedure involves two different energy consumptions—one is due to the injected energy to increase the PZT-clamped-capacitor voltage, and another is due to the resistive dissipation. Through using multiple voltage steps to directly charge the clamped capacitor, the dissipated energy by path resistance is reduced. Overall, due to the increased voltage level in PZT, during the next polarization current half cycle $(T/2)$, the harvested energy by PZT is significantly enhanced, resulting to a higher net power (harvested power minus the mentioned consumptions).

Now, in order to calculate the net output power under the voltage compensation scheme, we need the following: 1) the change in stored energy (injected energy) in the clamped capacitor during the application of voltage steps, which is given by

$$E_C = \frac{1}{2}C_p\left(V_2^2 - V_1^2\right) = \frac{1}{2}C_pV_2^2(1-\gamma^2) \tag{6}$$

2) the energy dissipation $E_{\rm DISS}$ in the current path according to

$$E_{\rm DISS} = \frac{1}{2\alpha}C_p(V_2 - V_1)^2 = \frac{1}{2\alpha}C_pV_2^2(1-\gamma)^2 \tag{7}$$

and 3) the harvested energy E_H during a half cycle $(T/2)$ at constant voltage V_2, which, due to negligible piezoelectric current at the time of inversion and compensation, can be calculated as

$$\begin{aligned} E_H &= \int_0^{T/2-(t_1+t_2+\pi\sqrt{LC_P})} I_P\sin(\omega t)V_2\,dt \\ &\approx \int_0^{\frac{T}{2}} I_P\sin(\omega t)V_2\,dt = \frac{2I_PV_2}{\omega} \end{aligned} \tag{8}$$

where $\gamma = |V_1/V_2|$ (which only depends on RLC circuit specifications), ω is the vibration angular frequency, and I_P is the maximum polarization current. By using the proposed topology, the maximum net output energy occurs when $d\Delta(E_H - E_C - E_{\rm DISS})/dV_2 = 0$, which yields $V_2 = I_P/K\omega C_P$, where $K(\alpha)$ is a design parameter as presented in [14] and V_2 and V_1 are the voltages before and after the switching, respectively, according to Fig. 3(a). Consequently, the maximum net power can be calculated as

$$P_{\rm MAX} = \frac{2}{T}\max(E_H - E_C - E_{\rm DISS}) = I_P^2/(K\pi\omega C_P). \tag{9}$$

D. Voltage Compensation in Series Inversion Technique

A scheme similar to the parallel voltage compensation is used in the series voltage compensation. The series topology [14] and that with the compensated voltage levels are shown

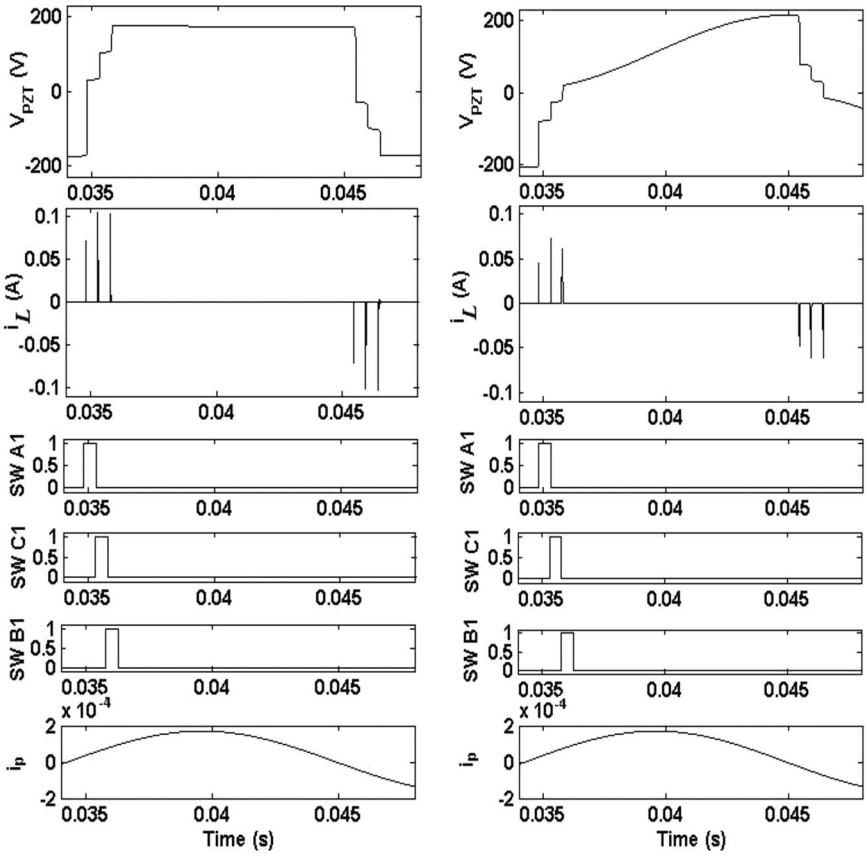

Fig. 4. Voltage and current waveforms. (a) Parallel voltage compensation topology. (b) Series voltage compensation topology. Pulse durations are bigger than those of lab tests for better graph quality.

in Figs. 2(b) and 3(b), respectively. The voltage starts to fall from V_2 to $-V_3$ because of inversion and during the transfer of energy to the load. At the end of the inversion, the piezoelectric clamped capacitor C_P is subjected to direct charging, and its voltage increases from $|-V_3|$ to $|-V_1|$ by voltage compensation through switches $C1$ and $B1$ at the beginning of the negative half cycle for two-step compensation ($C2$ and $B2$ for positive half cycle). This procedure is shown in Fig. 3(b) and is similar to the procedure shown in Fig. 3(a) for parallel compensation. Then, the switches are opened, and the piezoelectric polarization current source starts to transfer charge to the clamped capacitor.

Using the same logic as in the parallel voltage compensation, the maximum net output power in one-step compensation can be calculated using the procedure outlined in [14] as

$$P_{\mathrm{MAX}} = \frac{2}{T}\max(E_H - E_C - E_{\mathrm{DISS}}). \tag{10}$$

The maximum net output power happens when $V_1 = I_P\gamma/(C_P(1-\gamma)\omega)$ and $V_L = I_P/(C_P\omega)$, where $\gamma = |(V_3 + V_L)/(V_2 - V_L)|$ (which only depends on the RLC circuit specifications) and V_L is the load voltage [shown in Fig. 2(b)] and constant. Consequently, the maximum power is calculated as

$$P_{\mathrm{MAX}} = I_P^2/\left(\pi C_P(1-\gamma)\omega\right). \tag{11}$$

Operational voltages and current are shown in Fig. 3(b).

Fig. 4 shows the simulation results for PZT voltages and currents in parallel and series compensation schemes (for maximum power), as well as inversion and compensation switch signals.

III. Cantilever Beam Geometry

As mentioned before, a cantilever beam is widely used in piezoelectric energy harvesting mainly for its relatively low resonance frequency and high average strain for a given input force [15]. The rectangular and trapezoidal cantilever beam geometries and their strain profiles are compared in [15]. In order to render a larger portion of the bonded piezoelectric material to produce energy in [15], the trapezoidal beam is shown to produce twice the amount of energy (per unit volume PZT). However, the strain profile is still not uniform along the beam.

The uniform distribution of strain, which provides the maximum average strain, is obtained by taking into account the maximum tolerable strain of the material at each point along the tapered beam shown in Fig. 5. Such a curvature can be considered as the optimal, as long as it provides the maximum average strain for a given maximum tolerable strain. To the best of our knowledge, no such design has been introduced in the literature. Here, the detailed design and simplified design procedure, which relaxes math complexities in practical implementation, are introduced.

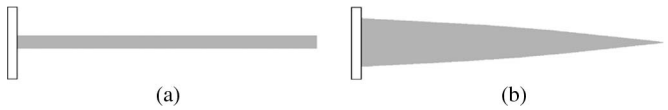

Fig. 5. (a) Rectangular beam. (b) Tapered beam.

A. Design Analysis

A tapered beam with a proof mass is shown in Fig. 6. The function $f_1(x)$ describes the distance between the surface area and the center of the cantilever beam, and $f_2(x) = f_1(x) + t_b/2$, where t_b is the piezoelectric material thickness. An enlarged picture of the beam's length is shown as the shaded area in Fig. 6(b). Using geometry, we know that

$$l^2 = (z+h)^2 + a^2 = b^2 + h^2 + 2zh. \tag{12}$$

According to the moment–area method [19]

$$z = \frac{M(x)}{EI(x)} \cdot \frac{\Delta x^2}{2} \tag{13}$$

where z is the displacement of the end point of bent element

$$M(x) = \frac{F}{EI(x)}\left(l_b + \frac{l_m}{2} - x\right) \tag{14}$$

with F as the force applied to the center of the proof mass, $I(x)$ as the moment of inertia given by

$$I(x) = 2\left(wt_P^3/12 + wt_P f_2^2(x)\right) + 2nwf_1^3(x)/3 \tag{15}$$

w as the width of the beam (and piezoelectric), and $n = E/E_S$, where E is the Young's modulus of the piezoelectric material and E_S is that of the metal beam.

Moreover, from Fig. 6(b), we have

$$h \approx |f_2'(x)|\,\Delta x \qquad b = \Delta x\left(1 + \frac{M(x)f_2(x)}{EI(x)}\right) \text{ [19]}. \tag{16}$$

Using (12)–(16), we have

$$l^2 = \Delta x^2\left[\left(1 + \frac{M(x)f_2(x)}{EI(x)}\right)^2 + \left(\frac{df_2(x)}{dx}\right)^2 + \frac{M(x)}{EI(x)}\frac{df_2(x)}{dx}\Delta x\right] \tag{17}$$

which can be approximated by

$$l^2 \approx \Delta x^2\left[\left(1 + \frac{M(x)f_2(x)}{EI(x)}\right)^2 + \left(\frac{df_2(x)}{dx}\right)^2\right]. \tag{18}$$

Defining l_P' as the length of the unbent curvature underneath the piezoelectric material, we have the average strain along the beam as

$$\varepsilon_{\text{ave}} = \frac{l - l_P'}{l_P'} = \frac{1}{l_P'}\left[\int_0^{l_P}\sqrt{\left(1 + \frac{M(x)f_2(x)}{EI(x)}\right)^2 + \left(\frac{df_2(x)}{dx}\right)^2}\,dx - l_P'\right]. \tag{19}$$

Moreover, the strain at each point along the beam can be obtained as

$$\varepsilon(x) = \left(\sqrt{\left(1 + \frac{M(x)f_2(x)}{EI(x)}\right)^2 + \left(\frac{df_2(x)}{dx}\right)^2} - \sqrt{1 + \left(\frac{df_2(x)}{dx}\right)^2}\right)\Bigg/\sqrt{1 + \left(\frac{df_2(x)}{dx}\right)^2}. \tag{20}$$

Knowing from the mechanics that

$$\varepsilon'(x) = \frac{M(x)f_2(x)}{EI(x)} \tag{21}$$

where $\varepsilon'(x)$ is the strain along the horizontal (before bending) flat surface b under the curved surface, as shown in Fig. 6(a) and (b), i.e., $\varepsilon'(x) = (b - \Delta x)/\Delta x$. Thus, it yields

$$\varepsilon(x) = \sqrt{1 + \left(\varepsilon'^2(x) + 2\varepsilon'(x)\right)/1 + \left(df_2(x)/dx\right)^2} - 1 = \varepsilon_{\text{CONST}} \tag{22}$$

where $\varepsilon_{\text{CONST}}$ is the desired constant strain along the beam.

By defining $(\varepsilon'^2(x) + 2\varepsilon'(x))/(1 + (df_2(x)/dx)^2) = K_1$, where $K_1 = (\varepsilon_{\text{CONST}} + 1)^2 - 1$ from (22), and after substituting for $\varepsilon'(x)$, we are able to solve (22) for $df_2(x)/dx$ as

$$\frac{df_2(x)}{dx} = \sqrt{\frac{2EF(l_T - x)I(x)f_2(x) + F^2(l_T - x)^2 f_2^2(x)}{K_1 E^2 I^2(x)} - 1} \tag{23}$$

where $l_T = l_b + l_m/2$.

In order to solve (23), a numerical approach has to be utilized. Moreover, an estimation of the applied force based on the source vibration frequency and vibration amplitude is needed for a solution. Note that, in the tapered beam, as x increases from zero to l_b, $f_2(x)$ decreases, which makes the momentum $M(x)$ larger, whereas in the rectangular beam, the momentum decreases when x increases. According to the bending energy $U = \int M^2/EIdx$ [19], large $M(x)$ along x gives higher energy concentration in the material, as well as higher α (defined in Section II), which, in turn, increases the PZT current i_P.

B. Design Simplification

Equation (23) reveals that, for the given E, F, l_T, $I(x)$, and K_1 at each point x along the beam, $f_2(x)$ is uniquely obtained if $df_2(x)/dx$ is known. For a smooth surface (i.e., continuous $f_2(x)$), (23) has to be solved, as described earlier; however, a discontinuous approximate solution is achievable, as described here. Comparing (21) and (22), we find that $\varepsilon(x) \leq \varepsilon'(x)$. In practice, the term $(df_2(x)/dx)^2$ in (22) is a small number (in our design, < 0.0009) such that we can assume that $\varepsilon(x) \approx \varepsilon'(x)$. This, in turn, reveals that the strain on the curved surface is equal to the strain on the flat surface underneath the curved surface shown in Fig. 6(b), provided that the length Δx is infinitesimal. Note that, on the flat surface, $df(x)/dx = 0$.

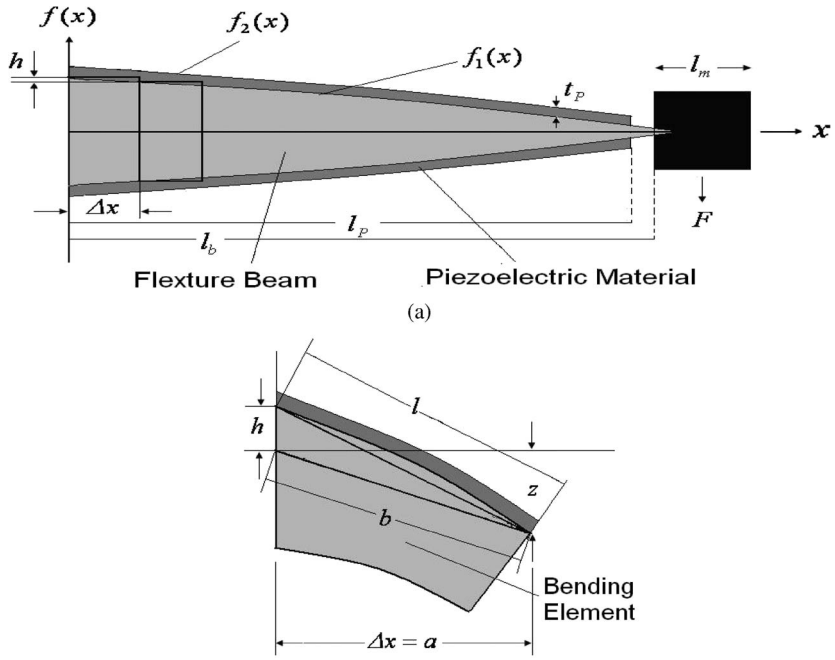

Fig. 6. (a) Tapered beam and its (b) bending element.

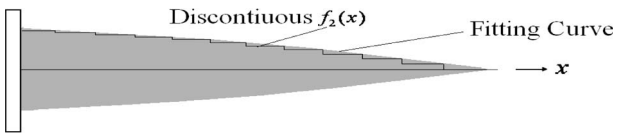

Fig. 7. Discontinuous design of $f_2(x)$ and fitting curve.

Given the desired constant strain along the beam $\varepsilon_{\mathrm{CONST}}$ and by assuming that $df_2(x)/dx = 0$ and solving (23) for $f_2(x)$ at each point x, a staircaselike surface is obtained with infinite numbers of steps.

By adopting limited number of points along the x-axis, an approximation to the staircase solution is achieved. The physical surface is made smooth by connecting the calculated $f_2(x)$'s via fitting a curve, as shown in Fig. 7, which by the same reasoning, has the same strain as the original curved surface represented by (23). Thus, adequately large number of points x ensures a good approximation of the actual solution for (23) since the staircaselike surface approaches the actual curve as the number of points goes to infinity.

IV. Simulation Results, Laboratory Results, and Field Test

The experimental setup consists of two 15-cm steel cantilever beams, namely, a rectangular beam and a tapered beam, both excited by a shaker. The tapered beam has been designed at 32 equally apart points along the beam, starting with $f_1(x) =$ 2 mm at the fixed point, using the simplified method. The designed tapered beam for the experimental tests is shown in Fig. 8(a). The simulation results of strain profiles with the tapered beam designed with the simplified method, as well as a rectangular beam, are given for the same maximum tolerable strain in Fig. 8(b).

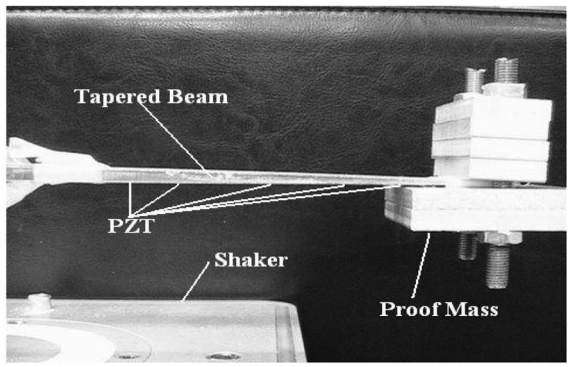

(a)

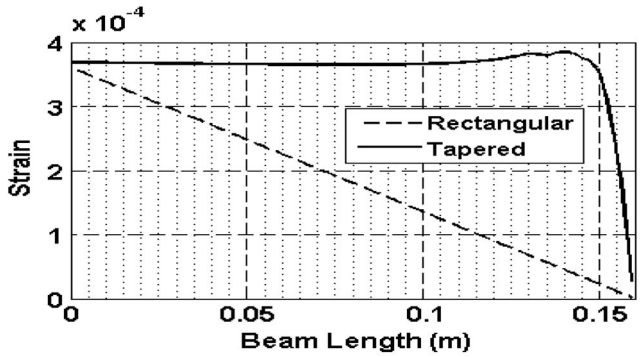

(b)

Fig. 8. (a) Designed tapered beam. (b) Simulation results: Strain profile along the rectangular and designed tapered beams using the simplified method.

The piezoelectric materials used are thin flexible strips of composite fibers with a laminate coating, which are glued on the cantilever beam using epoxy. The material specifications are shown in Table I. The internal capacitance of the piezoelectric material (one layer) was measured to be 2.8 nF using a conventional multimeter. When the PZT leads are connected to

TABLE I
PIEZOELECTRIC MATERIAL SPECIFICATIONS
(ADVANCED CERAMETRICS INC.)

Specifications	Values
Fiber Type	PZT-5A
Dimensions	13.0cmX1.0cmX0.4cm
Avg. Actual Strain @ 3KVpp under 600Vdc bias(ppm)	1800
Operational Voltage Limits	-1500 to 2800
Weight	1.8grams
Dielectric Constant at 1kHz	1725
K_{33}	72%
D_{33}	380(10e-12m/V)
Young's Modulus	6.6×10^{10} N/m^2

TABLE II
LABORATORY TEST SPECIFICATIONS FOR THE RECTANGULAR BEAM

	Parallel Compensation	Series Compensation
Frequency	40Hz	40Hz
Beam's free end no load vibration amplitude	4mm	4mm
I_P	$76\mu A$	$76\mu A$
C_P	$2.8nF$	$2.8nF$
Total capacitance seen from PZT terminals	$3.7nF$	$4.7nF$
γ	<0.5	<0.5
Maximum Standard DC Power	1.4mW	1.4mW

TABLE III
LABORATORY TEST SPECIFICATIONS FOR THE TAPERED BEAM

	Parallel Compensation	Series Compensation
Frequency	47Hz	47Hz
Beam's free end no load vibration amplitude	2.5mm	2.5mm
I_P	$170\mu A$	$170\mu A$
C_P	$2.8nF$	$2.8nF$
γ	<0.3	<0.3

the circuitry, the total capacitance seen from PZT terminals is not a constant but appears to be higher than 2.8 nF due to the capacitive effects of MOSFETs and measuring devices.

The polarization current I_P has been calculated using $V_P = I_P/C_P\omega$, where V_P is the open circuit peak voltage. The parameter γ has been measured using the voltage before and after inversion using oscilloscope and was varying occasionally. These values are given in Tables II and III. Moreover, $L = 10$ mH (2 A) is used, and MOSFETs are rated 500 V and 10-A instantaneous current.

Instead of voltage sources V_A, V_B, V_C, and V_D, the outputs of an adjustable flyback power converter ($P_{\rm MAX} = 100$ mW) have been used so that the compensated voltage can be adjusted by changing the switching frequency. However, equal voltage steps were not achieved due to the variation of load and PZT parameters. The voltage values $V_A + V_B$ and $V_C + V_D$ are kept slightly less than V_L (in parallel topology) to avoid direct charging of the rectifier capacitor. Due to the transient behavior of power transfer while directly charging the PZT-clamped capacitor C_P, the transferred charge Q_M from the compensating power supplies to the PZT during each compensation step has been measured using the change in voltage V_M (as measured by the oscilloscope), i.e., $Q_M = C_M \times \Delta V_M$, where $C_M = 0.1$ μF (100 V) is chosen.

Then, the transferred power from the power supplies to PZT is calculated by $P_m = 2/T \times (C_M \Delta V_{MA} V_A + C_M \Delta V_{MB}(V_A + V_B))$ and $P_m = 2/T \times (C_M \Delta V_{MC} V_C + C_M \Delta V_{MD}(V_C + V_D))$ for the negative and positive half cycles of PZT current i_P, respectively. The compensating voltages V_A, V_B, V_C, V_D, and $V_{\rm Load}$ have been measured using conventional multimeters. The net output power is defined as the difference between the load and the consumed (transferred) power.

In Fig. 9, the measured and theoretical power losses (for $C_P = 2.8$ nF) are compared, where the theoretical losses are calculated using $P_t = 2/T \times (C_P(V_2 - V_3)^2/2 + C_P(V_3 - V_1)^2/2) + 2/T \times (C_P V_2^2/2 - C_P V_1^2/2)$ in parallel topology (and using a similar relationship in the series topology.) The discrepancy between the experimental and theoretical values arises because the actual capacitance C_P is different from the PZT rated capacitance due to the effect of MOSFET output capacitances [9] (90 pF), as well as measuring device impedances. Moreover, we experienced noise while measuring V_1 in parallel topology and V_3 in series topology (for evaluating the theoretical values) using the oscilloscope due to equipment input impedance.

The load current shown in Fig. 10 in the series topology was a little lower than that of the parallel topology (which requires more investigation), although the mechanical vibration remained the same, and both decrease with voltage increase because of PZT induced force [9] on the beam. Also, in Figs. 10 and 11, the intermediate voltages, as well as the capacitor voltage V_M, are shown. The "Inversion Time" and "Step 1 and 2 Durations" (according to Fig. 3) were all less than 50 μs.

The experimental versus theoretical net powers for voltage compensation in parallel and series inversion methods are shown in Figs. 12 and 13 for the tapered and rectangular beams, respectively. According to these figures, experimental results match the theory with an acceptable accuracy at low voltages. However, at high voltages, they diverge due to the OFF-state losses of the solid-state switches and input resistance of the measuring devices. It is shown that the voltage compensation method with tapered beam provides 14% increase in the harvested power in parallel voltage inversion and about 75% in series voltage inversion method.

In addition, by using the same setup, a more powerful scavenger with the tapered beam is utilized, where the beam was then equipped with a double-layer PZT strip. Note that the optimal voltages introduced in Sections II-C and II-D remain the same if the volume of PZT is doubled since the proportion I_P/C_P remains constant. Accordingly, by using the proposed schemes and under the same test conditions including intermediate voltages as with one-layer PZT, 23 and 12 mW are obtained from parallel and series topologies, respectively. Moreover, in order to evaluate the obtained energy on a realistic scenario, a field setup has been arranged, which included the tapered beam with two double-layer PZT strips (four layers) glued on and underneath the beam.

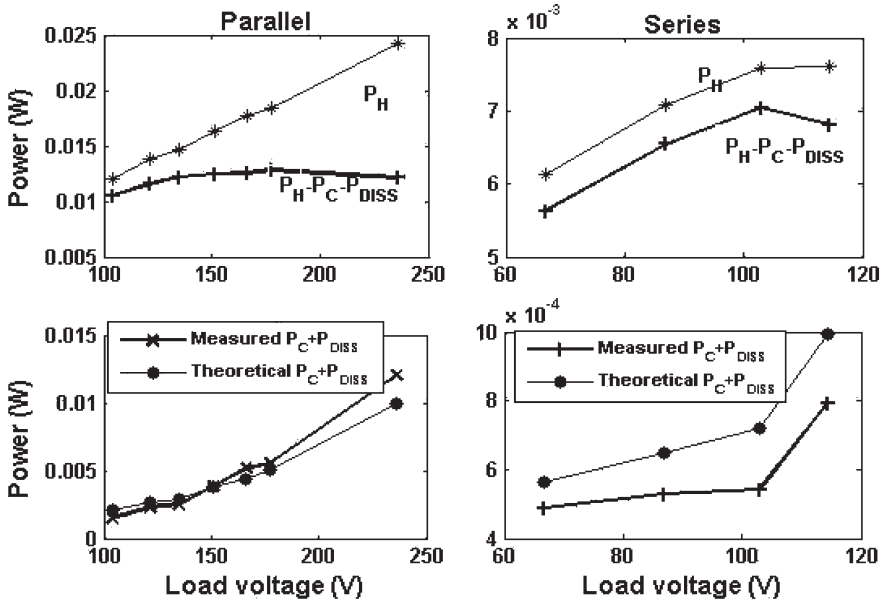

Fig. 9. Load power, net output power, and the dissipations for tapered beam.

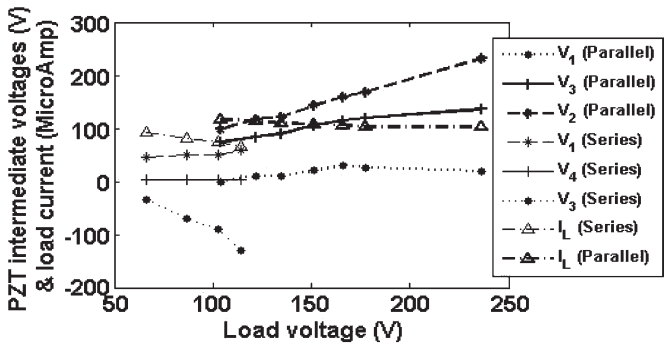

Fig. 10. Intermediate voltages and currents with the tapered beam, where V_4 is an intermediate step between V_3 and V_1.

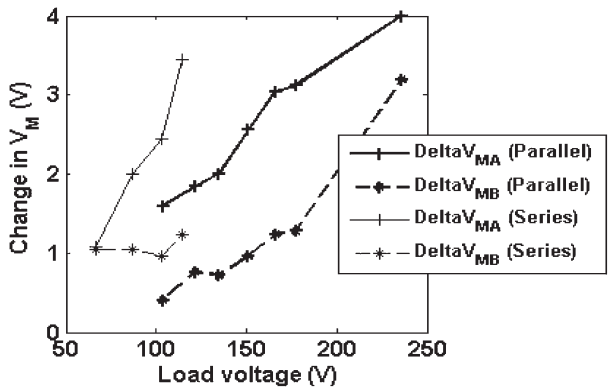

Fig. 11. Capacitor voltage V_M with the tapered beam.

The tapered beam was enclosed inside an enclosure, and it was mounted on a bulldozer, which was assumed to have adequate level of vibration while moving in a farm. The setup mounted on the bulldozer is shown in Fig. 14. The dc harvested power was measured using a wireless data acquisition system (Missouri S and T Mote). The data (harvested power) were then plotted with time, as shown in Fig. 15. According to the figure, an average dc harvested power of 5 mW is achievable from a

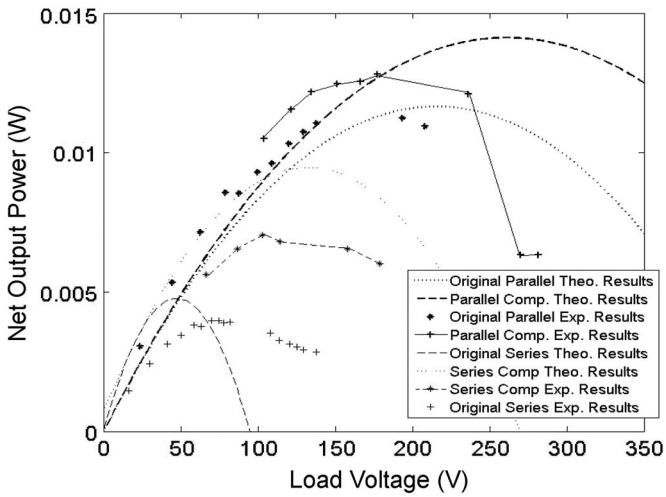

Fig. 12. Theoretical and lab results with the tapered beam for parallel and series compensation schemes, as well as original voltage inversion techniques.

moving bulldozer on an uneven rural field by using the tapered beam. However, in a mobile application, different frequencies, as well as shocks, are normally observed in contrast to a single frequency. Therefore, a multiple beam structure that resonates for a range of frequencies should be utilized as part of future work.

V. Conclusion

In voltage inversion techniques (also known as SSHI), the inversion process in a high-voltage scavenger will not be as efficient as that in low voltage since there appears to be a significant voltage drop after voltage inversion, which, in turn, decreases the efficiency of the harvesting method. By using the proposed voltage compensation scheme, the harvested power can be increased in both the parallel and series inversion scenarios compared to the case when such compensation is not used at all. Moreover, since a tapered cantilever beam appears to

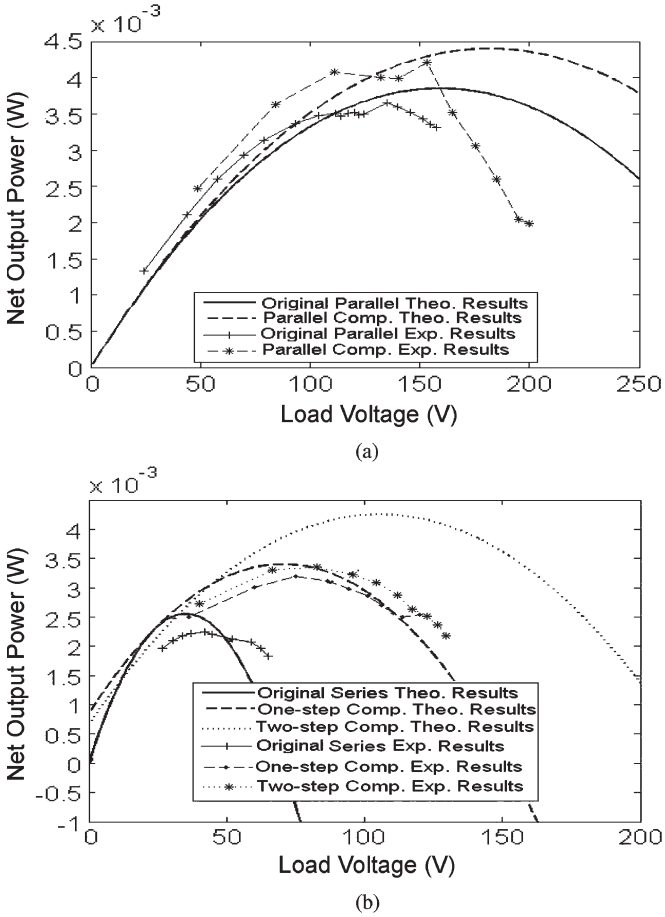

Fig. 13. Rectangular beam results. (a) Theoretical and experimental results using the parallel scheme. (b) Theoretical and experimental results using the series scheme.

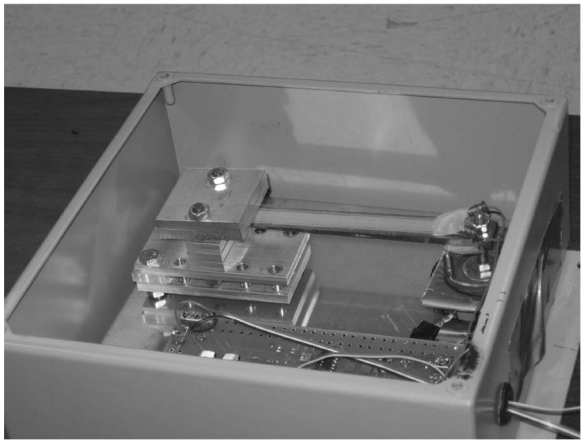

Fig. 14. Tapered beam field setup enclosure (size: 25 cm × 25 cm).

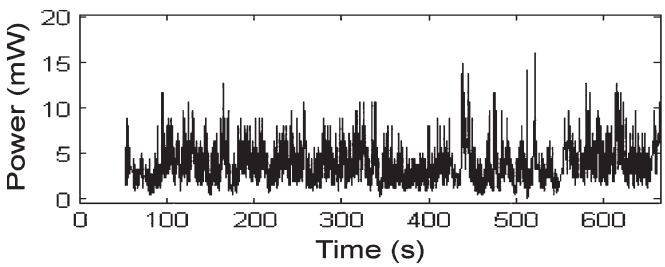

Fig. 15. Tapered beam power evaluation in the field.

produce more power, a simplified method of harvesting energy using a tapered beam has been included here. Laboratory and field trials have shown the validity of the proposed energy-harvesting method.

REFERENCES

[1] J. M. Carrasco, L. G. Franquelo, J. T. Bialasiewicz, E. Galvan, R. C. P. Guisado, M. A. M. Prats, J. I. Leon, and N. Moreno-Alfonso, "Power-electronic systems for the grid integration of renewable energy sources: A survey," *IEEE Trans. Ind. Electron.*, vol. 53, no. 4, pp. 1002–1016, Jun. 2006.

[2] J. Schonbergerschonberger, R. Duke, and S. D. Round, "DC-bus signaling: A distributed control strategy for a hybrid renewable nanogrid," *IEEE Trans. Ind. Electron.*, vol. 53, no. 5, pp. 1453–1460, Oct. 2006.

[3] M. E. Kiziroglou, C. He, and E. M. Yeatman, "Rolling rod electrostatic microgenerator," *IEEE Trans. Ind. Electron.*, vol. 56, no. 4, pp. 1101–1108, Apr. 2009.

[4] V. Raghunathan, A. Kansal, J. Hsu, J. Friedman, and M. Srivastava, "Design considerations for solar energy harvesting wireless embedded systems," in *Proc. IEEE 4th IPSN*, Apr. 15, 2005, pp. 457–462.

[5] R. Amirtharajah, J. Collier, J. Siebert, B. Zhou, and A. Chandrakasan, "DSPs for energy harvesting sensors: Applications and architectures," *Pervasive Comput.*, vol. 4, no. 3, pp. 72–79, Jul.–Sep. 2005.

[6] Y. K. Tan, K. Y. Hoe, and S. K. Panda, "Energy harvesting using piezoelectric igniter for self-powered radio frequency (RF) wireless sensors," in *Proc. IEEE ICIT*, Dec. 2006, pp. 1711–1716.

[7] J. Colomer-Farrarons, P. Miribel-Catala, A. Saiz-Vela, M. Puig-Vidal, and J. Samitier, "Power-conditioning circuitry for a self-powered system based on micro PZT generators in a 0.13-micro meter low-voltage low-power technology," *IEEE Trans. Ind. Electron.*, vol. 55, no. 9, pp. 3249–3257, Sep. 2008.

[8] B. H. Calhoun, D. C. Daly, V. Naveen, D. F. Finchelstein, D. D. Wentzloff, A. Wang, C. Seong-Hwan, and A. P. Chandrakasan, "Design considerations for ultra-low energy wireless microsensor nodes," *IEEE Trans. Comput.*, vol. 54, no. 6, pp. 727–740, Jun. 2005.

[9] D. Guyomar, A. Badel, E. Lefeuvre, and C. Richard, "Toward energy harvesting using active materials and conversion improvement by nonlinear processing," *IEEE Trans. Ultrason., Ferroelectr., Freq. Control*, vol. 52, no. 4, pp. 584–595, Apr. 2005.

[10] A. Badel, B. Benayad, E. Lefeuvre, L. Lebrun, C. Richard, and D. Guyomar, "Single crystals and nonlinear process for outstanding vibration-powered electrical generators," *IEEE Trans. Ultrason., Ferroelectr., Freq. Control*, vol. 53, no. 4, pp. 673–684, Apr. 2006.

[11] G. K. Ottman, H. F. Hofmann, and G. A. Lesieutre, "Optimized piezoelectric energy harvesting circuit using step-down converter in discontinuous conduction mode," *IEEE Trans. Power Electron.*, vol. 18, no. 2, pp. 696–703, Mar. 2003.

[12] G. K. Ottman, H. F. Hofmann, A. C. Bhatt, and G. A. Lesieutre, "Adaptive piezoelectric energy harvesting circuit for wireless remote power supply," *IEEE Trans. Power Electron.*, vol. 17, no. 5, pp. 669–676, Sep. 2002.

[13] K. Hyeoungwoo, S. Priya, H. Stephanou, and K. Uchino, "Consideration of impedance matching techniques for efficient piezoelectric energy harvesting," *IEEE Trans. Ultrason., Ferroelectr., Freq. Control*, vol. 54, no. 9, pp. 1851–1859, Sep. 2007.

[14] S. Mehraeen, S. Jagannathan, and K. Corzine, "Energy harvesting from vibration using high voltage scavenging circuitry," in *Proc. ICIT*, Apr. 2008, pp. 1–8.

[15] S. Roundy, E. S. Leland, J. Baker, E. Reilly, E. Lai, B. Otis, J. M. Rabaey, and P. K. Wright, "Improving power output for vibration-based energy scavengers," *Pervasive Comput.*, vol. 4, no. 1, pp. 28–36, Jan.–Mar. 2005.

[16] E. Hong, S. Trolier-McKinstry, R. Smith, S. V. Krishnaswamy, and C. B. Freidhoff, "Vibration of micromachined circular piezoelectric diaphragms," *IEEE Trans. Ultrason., Ferroelectr., Freq. Control*, vol. 53, no. 4, pp. 697–706, Apr. 2006.

[17] H. Xue, Y. Hu, and Q. Wang, "Broadband piezoelectric energy harvesting devices using multiple bimorphs with different operating frequencies," *IEEE Trans. Ultrason., Ferroelectr., Freq. Control*, vol. 55, no. 9, pp. 2104–2108, Sep. 2008.

[18] L. Garbuio, M. Lallart, D. Guyomar, C. Richard, and D. Audigier, "Mechanical energy harvester with ultralow threshold rectification based on SSHI nonlinear technique," *IEEE Trans. Ind. Electron.*, vol. 56, no. 4, pp. 1048–1056, Apr. 2009.

[19] F. P. Beer and E. R. Johnston, *Mechanics of Materials*. New York: McGraw-Hill, 1992.

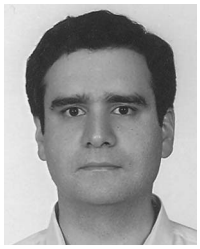

Shahab Mehraeen (S'08) received the B.S. degree in electrical engineering from Iran University of Science and Technology, Tehran, Iran, in 1995, the M.Sc. degree in electrical engineering from Esfahan University of Technology, Esfahan, Iran, in 2001, and the Ph.D. degree in electrical engineering from Missouri University of Science and Technology, Rolla, in 2009.

He is currently a Postdoctoral Fellow with Missouri University of Science and Technology. His research interests include renewable energies, power system control, decentralized control of large-scale interconnected systems and nonlinear, adaptive, and optimal controllers for dynamical systems.

S. Jagannathan (M'89–SM'99) received the B.S. degree in electrical engineering from the College of Engineering, Guindy, Anna University, Madras, India, in 1987, the M.Sc. degree in electrical engineering from the University of Saskatchewan, Saskatoon, SK, Canada, in 1989, and the Ph.D. degree in electrical engineering from The University of Texas in 1994.

During 1986 to 1987, he was a Junior Engineer with Engineers India Ltd., New Delhi, India, and a Research Associate and an Instructor at the University of Manitoba, Winnipeg, MB, Canada, from 1990 to 1991. He was with the Systems and Controls Research Division, Caterpillar Inc., Peoria, IL, as a Consultant from 1994 to 1998, and from 1998 to 2001, he was with The University of Texas, San Antonio. Since September 2001, he has been with the Missouri University of Science and Technology, Rolla, where he is currently the Rutledge-Emerson Distinguished Professor and the Site Director for the NSF Industry/University Cooperative Research Center on Intelligent Maintenance Systems. He has coauthored over 78 peer-reviewed journal articles, 150 IEEE conference articles, several book chapters, and three books entitled *Neural Network Control of Robot Manipulators and Nonlinear Systems* (Taylor and Francis, 1999), *Discrete-Time Neural Network Control of Nonlinear Discrete-Time Systems* (CRC Press, 2006), and *Wireless Ad Hoc and Sensor Networks: Performance, Protocols and Control* (CRC Press, 2007). He is the holder of 17 patents with several pending. His research interests include adaptive and neural network control, computer/communication/sensor networks, prognostics, and autonomous systems/robotics.

Dr. Jagannathan was the recipient of a 2000 NSF CAREER Award, the 2001 Caterpillar Research Excellence Award, the 2007 Boeing Pride Achievement Award, and many others. He served as an Associate Editor for the IEEE TRANSACTIONS ON NEURAL NETWORKS, IEEE TRANSACTIONS ON CONTROL SYSTEMS TECHNOLOGY, and IEEE SYSTEMS JOURNAL. He has also served on a number of IEEE Conference Committees.

Keith A. Corzine (S'92–M'97–SM'06) received the B.S.E.E., M.S.E.E., and Ph.D. degrees from Missouri University of Science and Technology, Rolla, in 1992, 1994, and 1997, respectively.

From 1997 to 2004, he was with the University of Wisconsin, Milwaukee. He is currently a Professor at Missouri University of Science and Technology, where he is also the Codirector of the Real-Time Power and Intelligent Systems Research Laboratory. His research interests include power electronics, motor drives, naval ship propulsion systems, and electric machinery. He has published over 30 refereed journal papers and over 50 refereed international conference papers and is the holder of two U.S. patents related to multilevel power conversion.

Dr. Corzine is currently the IEEE St. Louis Section Vice Chair and the St. Louis Section Industry Applications Society Chapter Cochair. He received the Faculty Excellence Award from Missouri University of Science and Technology in 2006 and the Excellence in Research Award from the University of Wisconsin in 2001.